Thermochimica Acta, 156 (1989) 259–266
Elsevier Science Publishers B.V., Amsterdam – Printed in The Netherlands

THE EFFECT ON HEAT FLUX DSC MEASUREMENTS OF PHYSICO-CHEMICAL PROPERTIES OF THE SAMPLE

A. MARINI, V. BERBENNI and V. MASSAROTTI

Centro di Studio per la Termodinamica CNR, Dipartimento di Chimica Fisica dell'Università di Pavia, Viale Taramelli 16, 27100 Pavia (Italy)

C. MARGHERITIS

Dipartimento di Chimica Inorganica dell'Università di Messina, 98100 Messina (Italy)

(Received 25 April 1989)

ABSTRACT

In order to account for the dependence of the calibration constant of a heat flux DSC cell on experimental variables and standard related properties, a study has been undertaken of the entire DSC trace. Part of this study has already been published.

The present report completes the general picture of the cell behaviour by defining the linkage between the measured signal and the relevant sample and experimental parameters. The proposed model is verified on the basis of the results of several calibration runs performed using different metal standards (In, Pb, Zn).

INTRODUCTION

In a previous work [1] dealing with the calibration of a heat flux DSC cell, it has been shown that the calibration constant depends both on the standard used and on experimental variables, e.g. the heating rate. In order to gain a thorough understanding of these relationships, a study was undertaken of the entire DSC trace.

Part of this study has already been published [2,3]. As regards the first half of the peak [2], analytical expressions were obtained for the rate of change of the temperature of both sample holder and reference holder. Moreover, it has shown that there exists a maximum signal value ΔT_{lim} which cannot be exceeded in the cell and which depends on experimental and instrumental parameters, but is independent of the physico-chemical properties of the sample. Analysis of the second half of the peak [3] provided an explanation as to why lower calibration constant values are obtained when the heating rate is increased.

In the present work, the general picture of the way in which a heat flux DSC cell works is completed through an assessment of the linkage between

0040-6031/89/$03.50

the measured signal and relevant physico-chemical properties of the sample, e.g. melting enthalpy and density. The experimental results of several calibration runs are then analysed on the basis of the proposed model.

Symbols and definitions are as used in ref. 2.

DISCUSSION

Since the sample temperature remains constant during melting, the total heat flux on the sample system (sample pan + the sample itself) will be utilized both as latent heat of fusion and as a heat source for increasing the temperature of the sample pan.

Thus we can write

$$(dQ/dt)_{s,f} = (dH/dt) + C_{p,Al}(dT_{Al,f}/dt) \tag{1}$$

where $C_{p,Al}$ is the aluminum sample pan thermal capacity, and $T_{Al,f}$ is the sample pan temperature during fusion.

Taking into account eqs. (6) and (10) of ref. 2, eqn. (1) becomes

$$(dQ/dt)_{R,f}\frac{(C_{pR}+C_{pRh})C_{ps}}{(C_{ps}+C_{psh})C_{pR}} + \beta(C_{ps}-C_{pR})\frac{C_{ps}}{(C_{ps}+C_{psh})} + \frac{(T_{Rhf}-T_{shf})C_{ps}}{R(C_{ps}+C_{psh})} = (dH/dt) + C_{p,Al}(dT_{Al,f}/dt) \tag{2}$$

However, the relationship

$$(dQ/dt)_{sf} = (T_{shf}-T_{Al,f})/R_3 = (T_{Al,f}-T_{s,f})/R_4 \tag{3}$$

must be fulfilled.

Differentiating eqn. (3) with respect to time and solving for $dT_{Al,f}/dt$, we obtain

$$dT_{Al,f}/dt = [R_4/(R_3+R_4)]\ (dT_{shf}/dt) \tag{4}$$

Equation (4) expresses the rate of change of the sample pan temperature during melting as a function of the rate of change of the sample holder temperature. Substituting eqn. (4) into eqn. (2), and taking into account eqn. (13) of ref. 2, we obtain

$$\left[(dQ/dt)_R - \frac{(T_{Rhf}-T_{shf})C_{pR}}{R_2(C_{pR}+C_{pRh})}\right]\frac{C_{ps}(C_{pR}+C_{pRh})}{C_{pR}(C_{ps}+C_{psh})} + \frac{(C_{ps}-C_{pR})C_{ps}\beta}{(C_{ps}+C_{psh})} + \frac{(T_{Rhf}-T_{shf})C_{ps}}{R(C_{ps}+C_{psh})} = (dH/dt) + C_{p,Al}\frac{R_4(dT_{shf}/dt)}{(R_3+R_4)} \tag{5}$$

Equation (5) relates the total heat flux on the sample system during melting (LHS) to the heat flux utilized as latent heat of fusion (first term of

RHS). However, our principal interest is with the relationship between the measured signal $T_{\mathrm{Rhf}} - T_{\mathrm{shf}}$ and the latent heat of fusion ΔH, so we need to determine the linkage between the 'differential' heat flux entering the sample system when melting occurs and the latent heat of fusion. This can be done by subtracting from the LHS and RHS of eqn. (5), respectively, the heat flux that would reach the sample system and the heat flux that would increase the sample pan temperature if no melting were to take place. The first of these values can be obtained using eqs. (7) and (9) of ref. 2, while the second is given simply by $C_{p,\mathrm{Al}}\beta$. The resulting equation is

$$\frac{\Delta T C_{ps}}{R_1(C_{ps}+C_{p\mathrm{sh}})} = (\mathrm{d}H/\mathrm{d}t) + C_{p,\mathrm{Al}}\left[\frac{R_4(\mathrm{d}T_{\mathrm{shf}}/\mathrm{d}t)}{(R_3+R_4)} - \beta\right] \tag{6}$$

Substituting into eqn. (6) for $(\mathrm{d}T_{\mathrm{shf}}/\mathrm{d}t)$ eqs. (15) and (17) of ref. 2, and taking into account the fact that $R_4 \ll R_2$ and $C_{p,\mathrm{Al}} < (C_{p\mathrm{R}} + C_{p\mathrm{Rh}})$, we obtain

$$\frac{C_{ps}\Delta T}{R_1(C_{ps}+C_{p\mathrm{sh}})} + \beta C_{p,\mathrm{Al}}\frac{R_1(C_{ps}+C_{p\mathrm{sh}}) + C_{ps}R_3}{R_1(C_{ps}+C_{p\mathrm{sh}}) + C_{ps}(R_3+R_4)} = (\mathrm{d}H/\mathrm{d}t) \tag{7}$$

Now $\mathrm{d}t$ can be expressed as a function of $\mathrm{d}\Delta T$ merely by rearranging eqn. (18) of ref. 2. Substitution of such an expression into eqn. (7) gives

$$\frac{C_{ps}\Delta T\left[R_1(C_{ps}+C_{p\mathrm{sh}}) + C_{ps}(R_3+R_4)\right]R_2(C_{p\mathrm{R}}+C_{p\mathrm{Rh}})}{R_1^2(C_{ps}+C_{p\mathrm{sh}})^2\left[\beta R_2(C_{p\mathrm{R}}+C_{p\mathrm{Rh}}) - \Delta T\right]}\mathrm{d}\Delta T$$
$$+ \frac{\beta C_{p,\mathrm{Al}}\left[(C_{ps}+C_{p\mathrm{sh}})R_1 + C_{ps}R_3\right]R_2(C_{p\mathrm{R}}+C_{p\mathrm{Rh}})}{R_1(C_{ps}+C_{p\mathrm{sh}})\left[\beta R_2(C_{p\mathrm{R}}+C_{p\mathrm{Rh}}) - \Delta T\right]}\mathrm{d}\Delta T = \mathrm{d}H \tag{8}$$

The term $\beta R_2(C_{p\mathrm{R}} + C_{p\mathrm{Rh}})$ represents the maximum signal value that can be established in the cell [2], while ΔT is the actual signal value generated by the melting process.

If $\Delta T \ll \beta R_2(C_{p\mathrm{R}} + C_{p\mathrm{Rh}})$, then eqn. (8) becomes

$$\frac{C_{ps}\Delta T\left[R_1(C_{ps}+C_{p\mathrm{sh}}) + C_{ps}(R_3+R_4)\right]}{\beta R_1^2(C_{ps}+C_{p\mathrm{sh}})^2}\mathrm{d}\Delta T$$
$$+ C_{p,\mathrm{Al}}\frac{\left[R_1(C_{ps}+C_{p\mathrm{sh}}) + C_{ps}R_3\right]}{R_1(C_{ps}+C_{p\mathrm{sh}})}\mathrm{d}\Delta T = \mathrm{d}H \tag{9}$$

which, by integration between the limits 0–$\Delta T_{\max}$ and 0–ΔH, gives

$$\frac{C_{ps}\left[R_1(C_{ps}+C_{p\mathrm{sh}}) + C_{ps}(R_3+R_4)\right]}{R_1^2(C_{ps}+C_{p\mathrm{sh}})^2\beta}(\Delta T_{\max}^2/2)$$
$$+ C_{p,\mathrm{Al}}\frac{R_1(C_{ps}+C_{p\mathrm{sh}}) + C_{ps}R_3}{R_1(C_{ps}+C_{p\mathrm{sh}})}\Delta T_{\max} = \Delta H_{\mathrm{peak}} = m\Delta H \tag{10}$$

where m is the sample mass, and ΔH is the sample melting enthalpy per unit mass.

Taking into account the fact that $R_1 \gg R_3 + R_4$, eqn. (10) becomes

$$\frac{C_{ps}\Delta T_{max}^2}{2\beta R_1(C_{ps} + C_{psh})} + C_{p,Al}\Delta T_{max} - m\Delta H = 0 \qquad (10')$$

from which ΔT_{max} can be obtained using

$$\Delta T_{max} = \frac{-C_{p,Al}\beta R_1(C_{ps} + C_{psh})}{C_{ps}} + \left[\frac{\beta^2 R_1^2(C_{ps} + C_{psh})^2 C_{p,Al}^2}{C_{ps}^2} + \frac{2m\Delta H\beta R_1(C_{ps} + C_{psh})}{C_{ps}}\right]^{1/2} \qquad (10'')$$

Equation (10″) links the maximum temperature difference in the cell (i.e. the maximum signal value) which is due to fusion with the melting enthalpy. From this relationship it can be seen that the maximum temperature difference depends on both ΔH and β.

Comparison of the dependences of ΔT_{max} and ΔT_{lim} on the experimental parameters ΔH and β can now explain why these parameters can affect the quantitative results.

It was shown in ref. 2 that the peak slope and the maximum signal value ΔT_{lim} allowed to be generated in the cell can be expressed as

$$(d\Delta T/dt) = \beta - \left[\frac{\Delta T}{R_2(C_{pr} + C_{pRh})}\right]$$

$$\Delta T_{lim} = \beta R_2(C_{pR} + C_{pRh})$$

It can be easily seen, as a general observation, that the peak slope decreases as ΔT (and then ΔT_{max}) approach ΔT_{lim}. This results in a peak shape which is different from the straightforward ideal case ($\Delta T_{max} \ll \Delta T_{lim}$), and consequently in a smaller peak area. Now when the heating rate is increased, ΔT_{lim} increases as β while ΔT_{max} increases as β^n ($0 < n < 0.5$, depending on the relative weights of the two terms in square brackets of the RHS of eqn. (10″)). It follows that, providing other factors remain constant, the difference between ΔT_{lim} and ΔT_{max} increases, leading to a situation where the peak area approaches the ideal (Fig. 1).

With increasing m or ΔH, however, ΔT_{max} increases as $(m\Delta H)^n$, with $0.5 < n < 1$, while ΔT_{lim} does not. The difference between ΔT_{lim} and ΔT_{max} decreases, which leads to a peak area smaller than that for the ideal case (Fig. 2), and to calibration constants higher than the correct ones.

Table 1 reports the calibration constant values obtained for different metal standards at heating rates of 1, 10 and 100 K min^{-1}. It can be seen that the calibration constant values obtained using each standard decrease

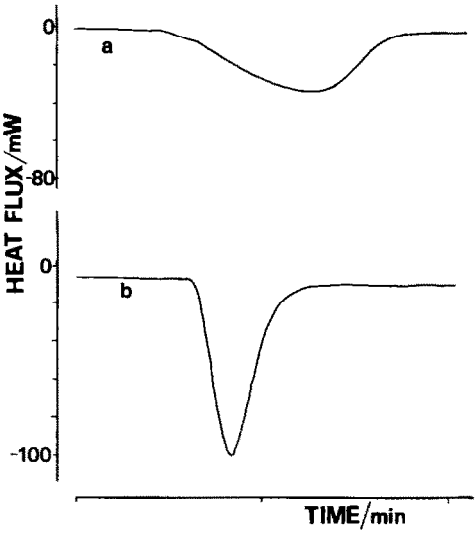

Fig. 1. Melting peaks of a zinc sample (15.7 mg): (a) heating rate, 10 K min^{-1}; b) heating rate, 100 K min^{-1}. Each division of the x-axis corresponds to 1 min. It can be seen that, as a consequence of the higher heating rate, peak b differs from peak a in that it has a nearly constant slope (first half of the peak), meaning that it approaches ideal shape and area more closely than does peak a.

with increasing heating rate. This experimental behaviour has been previously accounted for [3] by showing that, other experimental conditions being fixed, the area of the second half of the peak increases with increasing heating rate, thus leading to lower calibration constants. Here the picture of the way in which heating rate affects the quantitative response of the cell is completed.

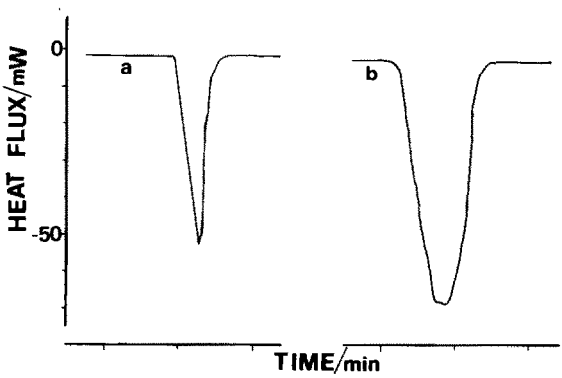

Fig. 2. Melting peaks of two different standards at the same heating rate (10 K min^{-1}): (a) indium, 65.4 mg; (b) zinc, 65.6 mg. Each division of the x-axis corresponds to 2 min. It can be seen that, owing to the lower melting enthalpy, peak a approaches ideal shape and area more closely than does peak b.

TABLE 1

Calibration constant values (dimensionless) obtained at different heating rates using different metal standards [a]

Heating rate (K min^{-1})	Calibration constant		
	Indium	Lead	Zinc
1.0	1.244	1.336	1.344
10.0	1.201	1.315	1.330
100.0	1.186	1.235	1.249
ΔH [b] ($J g^{-1}$)	28.4	24.6	112.0

[a] Each value was obtained as a mean of several measurements performed on different samples.

[b] ΔH represents the melting enthalpy per unit mass (see text for discussion).

In fact, as has been shown, an increasing heating rate may be thought of as counteracting the influence of the ΔH parameter on the peak area. This could explain why the differences between the calibration constant values obtained using different standards decrease with increasing heating rate (see Table 1 for heating rates of 1 and 100 K min^{-1}). On the other hand, when results obtained using different standards are analysed, higher calibration constant values are expected with increased sample melting enthalpy per unit mass.

Table 1 shows that this is verified for zinc but not for lead. The melting enthalpy of lead is close to that of indium, but lead gives calibration constant values close to those obtained with zinc. Some other sample related property has therefore to be taken into account to explain the experimental results.

As the heat is flowing from the pan to the sample, the heat flux per unit time depends on how much of the bottom surface of the pan is covered by the sample, and it will therefore reach its maximum value when the pan bottom is fully covered by the sample.

Thus eqn. (19) of ref. 2 should be rewritten (neglecting for the sake of simplicity the second term of the RHS) as

$$d\Delta T/dt = \beta S_s/S_{Al} \tag{11}$$

where S_s is the surface of the pan bottom covered by the sample, and S_{Al} is the geometrical surface of the bottom of the pan.

Now

$$S_s = m/dh;\ S_{Al} = m_0/dh$$

where m is the sample mass, m_0 is the sample mass needed to fully cover the geometrical surface of the bottom of the pan, h is the height of the sample layer, and d is the sample density.

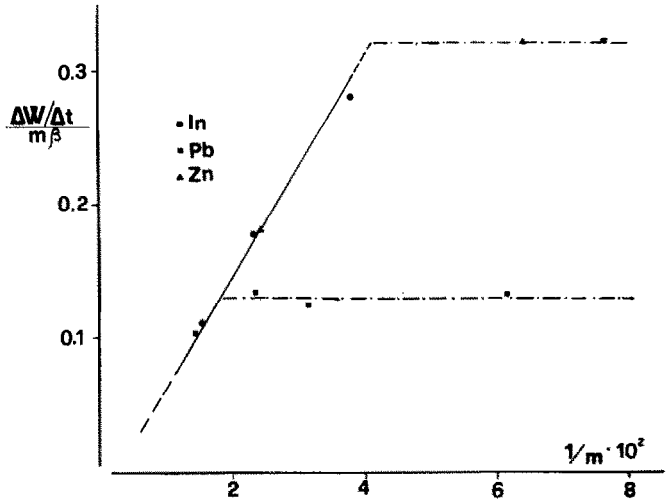

Fig. 3. Normalized heat flux (mW mg^{-1} K^{-1}) vs. $1/m$ (mg^{-1}). Points are representative of measurements performed at different heating rates and with different sample masses.

It follows that $S_s/S_{Al} = m/m_0$, and eqn. (11) becomes

$$d\Delta T/dt = \beta m/m_0 \tag{12}$$

which, after integration, can be written in the form

$$(\Delta T/\Delta t)/\beta = (m/m_0) \tag{12'}$$

Now, as $(\Delta T/\Delta t) = R(\Delta W/\Delta t)$ (see ref. (2) for the meaning of R and of $\Delta W \equiv (dQ/dt)_{shf} - (dQ/dt)_{Rhf}$), eqn. (12') can be written as

$$(\Delta W/\Delta t)/\beta = (m/m_0)(1/R) \tag{12''}$$

Equation (12'') only holds for $m \leqslant m_0$, and shows that the heat flux per unit time and unit heating rate increases with increasing m, so that when normalized with respect to m, it becomes mass independent.

When $m = m_0$, eqn. (12'') becomes

$$(\Delta W/\Delta t)/\beta = 1/R \tag{12'''}$$

showing that the heat flux per unit time and unit heating rate reaches a maximum value, so that when normalized with respect to m, it decreases with increasing sample mass.

Figure 3 confirms our predictions. Here the heat flux per unit time, unit mass and unit heating rate is reported for each standard as a function of the reciprocal mass $1/m$. Points for each standard lie on straight lines parallel to the abscissa axis (see eqn. (12'')) up to a threshold mass value m_0 which depends on the standard density. For larger mass values, by contrast, the normalized heat flux becomes mass dependent, and points for each standard lie, as expected, on the same straight line.

As noted, the intersection points between the straight lines representing the varying behaviour of the normalized heat flux with respect to sample mass depend on the standard density, lower intersection values corresponding to higher densities (lead in the present case).

Therefore, the 'anomalous' calibration constant values obtained from lead can be explained by taking into account its high density with respect to that of indium: lead will provide a smaller than expected signal value, and thus a higher than expected calibration constant value.

REFERENCES

1 A. Marini, V. Berbenni, V. Massarotti, G. Flor and G. Campari Viganò, Thermochim. Acta, 85 (1985) 279.
2 A. Marini, V. Berbenni, G. Flor, V. Massarotti and R. Riccardi, Thermochim. Acta, 95 (1985) 419.
3 A. Marini, V. Berbenni, V. Massarotti and G. Flor, J. Therm. Anal., 33 (1988) 337.